2014 IEEE International Conference on Robotics & Automation (ICRA)
Hong Kong Convention and Exhibition Center
May 31 - June 7, 2014. Hong Kong, China

Mechanical Implementation of Postural Synergies Using a Simple Continuum Mechanism

Kai Xu*, *Member, IEEE*, Huan Liu, *Student Member, IEEE*, Yuheng Du,
Xinjun Sheng, Member, IEEE, and Xiangyang Zhu, Member, IEEE

***Abstract*—It is known that human controls muscles for hand poses in a coordinated manner and the coordination is referred to as a postural synergy. Using postural synergies, dexterous grasping tasks could be accomplished on a prosthetic hand via only a few (usually two) control inputs. Instead of implementing postural synergies digitally, this paper presents the design of a simple continuum mechanism for implementing the postural synergies mechanically. The design, fabrication and assembly of a prosthetic hand are firstly presented, followed by the synthesis of postural synergies from various grasping poses. Referring to the extracted postural synergies, structural parameters of the continuum mechanism are calculated based on a kinematics model. Experimental verifications are also presented to demonstrate the efficacy of the proposed idea.**

I. Introduction

BUILDING an anthropomorphic versatile prosthetic hand is a challenging task. The design should be dexterous enough for various daily tasks and controllable through a bio-signal interface, such as EMG (electro-myography) or EEG (electro-encephalography). However the bandwidth of these interfaces is too limited to allow individual control of each joint on a fully actuated robotic hand.

Findings in neurology showed that CNS (Central Nervous System) controls hand muscles in a coordinated manner. This coordination is referred to as a postural synergy [1]. Each postural synergy represents the flexion or extension statuses of a group of muscles. CNS combines the postural synergies to realize various hand motions by adjusting each synergy's weight. Combination of the two primary postural synergies accounts for 84% of the variance of dozens of different grasping poses [2]. Furthermore, CNS switches between different sets of postural synergies for distinct grasping tasks [3].

These findings enabled the control of a fully-actuated robotic hands via a few (usually two to three) inputs, potentially allowing the state-of-the-art ones [4-7] to be applied as prostheses. These inputs could be decoded from an amputee's bio-signal interface and act as coefficients while combining the postural synergies. For example, two synergies are used to control 12 motors of the DLR II Hand for various grasping tasks [8], whereas two synergies are used to drive 20 actuators of the UB Hand IV [9]. Three synergies are used to control 13 motors of the SAH hand [10], whereas two and three postural synergies are used to control 24 motors of the ACT hand for writing and piano playing [11, 12].

The concept of postural synergies provides an alternative understanding of hand motion atlas to the discrete grasp taxonomy as in [13-15]. What's more, grasping planning could also be facilitated as shown in a milestone work by Ciocarlie and Allen [16].

A popular approach adopted by many designs [8-12] is to design a fully-actuated robotic hand and implement postural synergies digitally in the controller. This approach is convenient for implementing and switching between several groups of synergies. But the hand would be complex and expensive with multiple sets of miniature servomotors with amplifiers, feedback sensors and the controller. If postural synergies could be mechanically implemented, such a prosthetic hand could potentially be more affordable.

Mechanical implementation of the postural synergies was attempted by Brown and Asada using differential pulleys [17] and by Xu *et al.* [18, 19] using planetary gears. Both options are feasible in terms of realizing the synergies. But neither option can be easily further miniaturized for practical uses. This paper proposes to use a simple continuum structure for the mechanical implementation of the postural synergies. The proof-of-concept prototype is shown in Fig. 1. The sparse arrangement of the structural members in the continuum mechanism leaves us a possibility for further miniaturization.

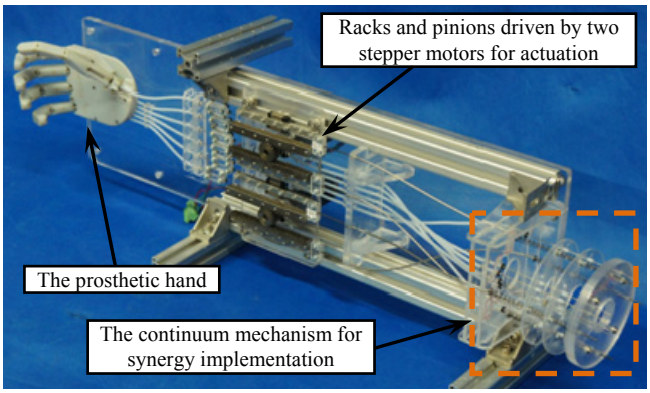

Fig. 1. A prosthetic hand with a simple continuum structure as the mechanical implementation of its postural synergies

Manuscript received Sept 15*th*, 2013. This work was supported in part by the National Program on Key Basic Research Projects (Grant No. 2011CB013300), in part by the Science and Technology Commission of Shanghai Municipality (Grant No. 13430721600), and in part by the National Natural Science Foundation of China (Grant No. 51375296).

Kai Xu, Huan Liu and Yuheng Du are with the RII Lab (Lab of Robotics Innovation and Intervention), UM-SJTU Joint Institute, Shanghai Jiao Tong University, Shanghai, 200240, China (asterisk indicates the corresponding author, phone: 86-21-34207220; fax: 86-21-34206525; emails: k.xu@sjtu.edu.cn, jhdyh1991@sjtu.edu.cn, and liuhuan_2013@sjtu.edu.cn).

Xinjun Sheng and Xiangyang Zhu are with the School of Mechanical Engineering, Shanghai Jiao Tong University, Shanghai, China (emails: xjsheng@sjtu.edu.cn and mexyzhu@sjtu.edu.cn).

The main contribution of this paper is the proposal of using continuum mechanisms for mechanical implementation of the postural synergies. The minor contribution is a specific design of such a continuum mechanism which realizes the combination of two postural synergies. The future goal is to design a continuum mechanism, which can be completely imbedded in a palm, for the synergy implementations.

The paper is organized as follows. Section II presents the design of a prosthetic hand and the synthesis of the postural synergies. Section III presents the kinematics of the simple continuum mechanism and the dimension synthesis for the synergy implementation. Section IV presents experimental validations with the conclusions and the future work followed in Section V.

II. Hand Design and Synergy Synthesis

Postural synergy synthesis involves the extraction of the principle components of various grasping poses. Instead of inviting 5 to 10 human subjects, asking them to perform the desired grasping tasks, recording and analyzing the human hand motions using fancy systems such as CyberGlove™ or Vicon™ cameras, this paper proposes to extract postural synergies directly from the grasping poses of a fabricated prosthetic hand. This idea was also practiced in [8].

The design, fabrication and assembly of an underactuated prosthetic hand are presented in Section II.A, whereas Section II.B presents the synergy synthesis.

A. Descriptions of the prosthetic hand

As shown in Fig. 2, the underactuated prosthetic hand has 16 joints, including 4 joints for the thumb and 3 joints for each finger. As indicated in Fig.2(a), Letters *T* and *I* before the underscore indicate the joints for the thumb and the index finger. Abbreviations of *rot*, *mcp*, *ip*, *abd*, *pip* and *dip* indicate the rotation joint, the metacarpophalangeal joint, the interphalangeal joint, the abduction joint, the proximal and the distal interphalangeal joint respectively.

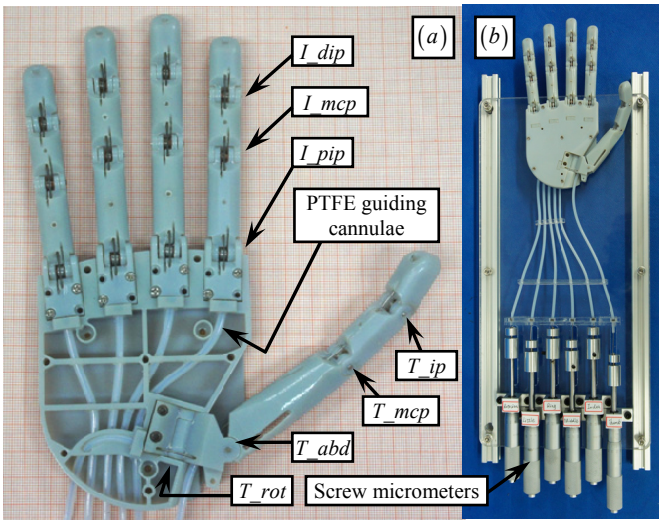

Fig. 2. Design of the underactuated prosthetic hand: (a) the assembly and (b) the hand with six screw micrometers as push-pull actuators

The 16 joints are actuated by 6 NiTi (nickel-titanium alloy) super-elastic thin rods. Diameter of the NiTi rod is 0.7mm.

Each finger is actuated by one NiTi rod. As shown in Fig. 3, the NiTi rod is attached to the distal phalange of the index finger. Then the NiTi rod is routed through the channels in the intermediate phalange and the proximal phalange towards the palm. The rod is passed through a PTFE guiding cannulae (outer diameter 3.0mm and inner diameter 1.0mm) all the way to a screw micrometer as shown in Fig. 2(b).

By manually rotating the screw micrometer, the NiTi rod would be pulled or pushed to close or open the index finger. Torsional springs are included for the *I_pip*, the *I_mcp* and the *I_dip* joints to allow approximately equal rotation angles of the three coupled joints when the NiTi rod is pulled.

The middle, the ring and the little fingers have structures and actuation schemes similar to those of the index finger.

The thumb is actuated by two NiTi rods. One NiTi rod actuates the *T_rot* joint while the other actuates the *T_abd*, the *T_mcp* and the *T_ip* joints. The NiTi rods are again routed through PTFE guiding cannulae to the screw micrometers for the actuation of the thumb.

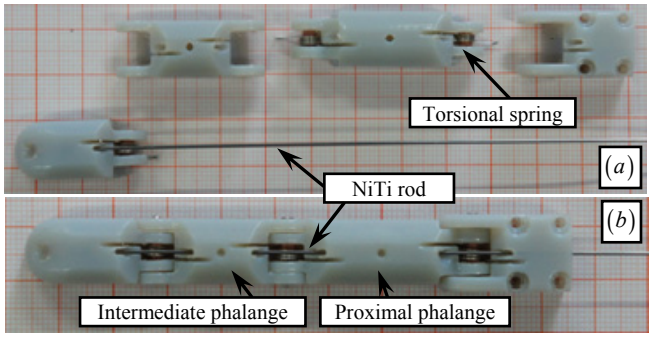

Fig. 3. The index finger of the prosthetic hand: (a) parts and (b) assembly

B. Postural synergy synthesis

Postural synergies are usually extracted as the first a few (usually two) principal components from the recorded joint angles of a hand under various grasping poses.

Instead of recording individual joint angles, this paper proposes to directly record the push-pull actuation lengths for synergy synthesis. The synergy values with a unit of length could be directly used for dimension determination of the continuum mechanism as described in Section III.B

The six screw micrometers are manually driven to push or pull the NiTi rods to let the hand form various grasping poses. The measured actuation lengths for the ten poses are listed in Table I. The values in the *T_rot* column means the actuation lengths for the *T_rot* joint, whereas the values in the *Thumb* column means the actuation lengths for the coupled *T_abd*, *T_mcp* and *T_ip* joints. The rest columns list actuation lengths for the index, the middle, the ring and the little fingers. A zero mm of these actuation lengths corresponds to the fully extended pose of the hand. Some poses are shown in Fig. 4.

Each pose can be written as a pose vector $\mathbf{p}_i \in \Re_{6\times 1}$ ($i = 1,2,\cdots,10$), whose elements are corresponding actuation lengths. The ten poses can be put side to side to form a pose matrix $\mathbf{P}$. Singular value decomposition can be performed on this pose matrix:

$$\mathbf{P}_{6\times10} = [\mathbf{p}_1 \quad \mathbf{p}_2 \quad \cdots \quad \mathbf{p}_{10}] = \bar{\mathbf{P}} + \mathbf{U}_{6\times6}\boldsymbol{\Sigma}_{6\times10}\mathbf{V}^T_{10\times10} \qquad (1)$$

Where $\bar{\mathbf{P}} = [\bar{\mathbf{p}} \quad \bar{\mathbf{p}} \quad \cdots \quad \bar{\mathbf{p}}]$ is the average pose matrix, $\bar{\mathbf{p}} = \frac{1}{10}\sum_{i=1}^{10}\mathbf{p}_i$ and $\mathbf{U} = [\mathbf{u}_1 \quad \mathbf{u}_2 \quad \cdots \quad \mathbf{u}_6]$.

If only the first two principle components are kept, each pose can be approximated as follows:

$$\mathbf{p}_i \approx \bar{\mathbf{p}} + g_{1i}\mathbf{u}_1 + g_{2i}\mathbf{u}_2\,,\ i = 1,2,\cdots,10 \qquad (2)$$

The numerical values of $\mathbf{u}_1$ and $\mathbf{u}_2$ are also listed in Table I with corresponding g_{1i} and g_{2i} values. $\mathbf{u}_1$ and $\mathbf{u}_2$ can be directly used to determine the structural parameters of the continuum mechanism as presented in Section III.B.

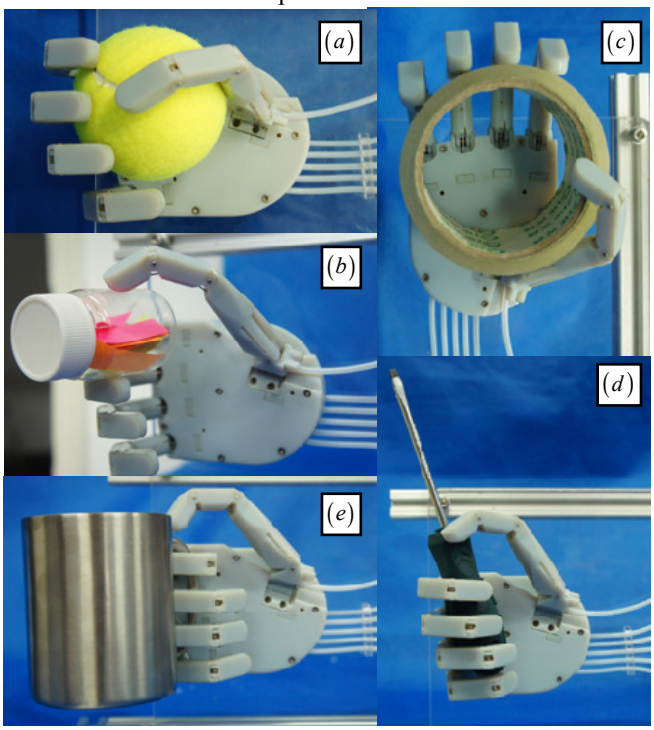

Fig. 4. Grasping poses for synergy synthesis: (a) a tennis ball, (b) a pill jar, (c) a roll of tape, (d) a screwdriver and (e) a mug

TABLE I
NITI ROD ACTUATION LENGTHS (UNIT: MILLIMETER) AND SYNERGIES

Poses	T_rot	Thumb	Index	Middle	Ring	Little
Tennis ball	12.00	13.38	17.68	18.25	18.04	20.09
Book	12.15	9.31	14.68	17.59	17.97	20.71
Cup	14.09	12.45	15.05	17.71	17.55	15.95
Pill jar	6.94	14.35	16.73	20.39	20.42	20.33
Box	6.27	15.52	18.98	23.45	22.38	22.31
Tape	7.61	16.40	15.21	16.71	16.59	16.46
Can	13.11	12.93	16.75	18.52	17.45	16.80
Screwdriver	1.77	18.84	28.80	30.36	31.50	27.90
Bottle	11.71	14.61	15.75	19.33	20.07	17.98
Mug	1.37	18.37	36.04	34.30	32.05	34.35
$\mathbf{u}_1 = [-0.32 \ \ 0.17 \ \ 0.54 \ \ 0.46 \ \ 0.43 \ \ 0.43]^T$						
$\mathbf{u}_2 = [0.68 \ \ -0.58 \ \ 0.27 \ \ 0.07 \ \ -0.03 \ \ 0.35]^T$						
	g_{1i}	g_{2i}		g_{1i}	g_{2i}	
Tennis ball	-5.80	1.9	Tape	-8.11	-4.84	
Book	-8.22	3.72	Can	-8.28	1.53	
Cup	-10.28	1.65	Screwdriver	19.08	-2.04	
Pill jar	-2.43	-2.20	Bottle	-6.07	-0.28	
Box	2.30	-1.88	Mug	27.82	2.45	

III. SYNERGY IMPLEMENTATION USING A CONTINUUM MECHANISM

This paper proposes to implement the postural synergy mechanically. In other words, a mechanical system shall be designed to realize linear combination of the two postural synergies under different weights (or called synergy inputs). Mechanical implementation of the postural synergies was previously attempted by Brown and Asada using differential pulleys [17] and by Xu *et al.* [18, 19] using planetary gears.

This paper proposes to use a simple continuum mechanism to implement the postural synergies. Structure of the continuum mechanism is shown in Fig. 5. It consists of an end disk, several secondary backbones, a few spacer disks and a base disk. All the backbones are made from thin NiTi super-elastic rods. The secondary backbones are only attached to the end disk and can slide in holes of the spacer disks and the base disk. A virtual primary backbone is assumed to be at the center and it characterizes length and shape of the continuum mechanism.

Among the secondary backbones in Fig. 5, four driving backbones are arranged at the outermost positions in the mechanism and several driven backbones are arranged at various inside positions. Push-pull actuations of the driving backbones will actively bend the continuum mechanism. Bending of the mechanism will lead to translational outputs from the driven backbones.

Kinematics of this mechanism will be derived in Section III.A and dimension determination according to the specific postural synergy values are presented in Section III.B.

A. Nomenclature and Kinematics

Nomenclatures are defined in Table II, while coordinate systems are defined as follows.

- *Base Disk Coordinate System* (BDS) is designated as $\{b\} \equiv \{\hat{\mathbf{x}}_b, \hat{\mathbf{y}}_b, \hat{\mathbf{z}}_b\}$. It is attached to the base disk of the continuum mechanism, whose XY plane coincides with the base disk and its origin is at the center. $\hat{\mathbf{x}}_b$ points from the center to the first secondary backbone while $\hat{\mathbf{z}}_b$ is normal to the base disk. Secondary backbones are numbered according to the definition of δ_i.
- *Bending Plane Coordinate System 1* (BPS1) is designated as $\{1\} \equiv \{\hat{\mathbf{x}}_1, \hat{\mathbf{y}}_1, \hat{\mathbf{z}}_1\}$ which shares its origin with $\{b\}$ and has the virtual primary backbone of the continuum structure bending in its XZ plane.
- *Bending Plane Coordinate System 2* (BPS2) is designated as $\{2\} \equiv \{\hat{\mathbf{x}}_2, \hat{\mathbf{y}}_2, \hat{\mathbf{z}}_2\}$ obtained from $\{1\}$ by a rotation about $\hat{\mathbf{y}}_1$ such that $\hat{\mathbf{z}}_1$ becomes backbone tangent at the end disk. Origin of $\{2\}$ is at center of the end disk.
- *End Disk Coordinate System* (EDS) $\{e\} \equiv \{\hat{\mathbf{x}}_e, \hat{\mathbf{y}}_e, \hat{\mathbf{z}}_e\}$ is fixed to the end disk. $\hat{\mathbf{x}}_e$ points from center to the 1*st* secondary backbone and $\hat{\mathbf{z}}_e$ is normal to the end disk. $\{e\}$ is obtained from $\{2\}$ by a rotation about $\hat{\mathbf{z}}_2$.

TABLE II
NOMENCLATURE USED IN THIS PAPER

m	Number of the secondary backbones
i	Index of the secondary backbones, $i = 1,2,\cdots,m$
r_i	Distance from the virtual primary backbone to the i*th* secondary backbone.
β_i	β_i characterizes the division angle from the i*th* secondary backbone to the 1*st* secondary backbone. $\beta_1 \equiv 0$ and β_i remain constant once the mechanism is built.
L, L_i	Lengths of the virtual primary and the i*th* secondary backbones measured from the base disk to the end disk.
d_i	Diameter of the i*th* secondary backbone
$\rho(s), \rho_i(s_i)$	Radius of curvature of the primary and the i*th* secondary backbones.
$\mathbf{q}$	$\mathbf{q} = [q_1 \ q_2 \ \cdots \ q_m]^T$ is the actuation lengths for the secondary backbones and $q_i \equiv L_i - L$.
$\theta(s)$	The angle of the tangent to the virtual primary backbone in the bending plane. $\theta(L)$ and $\theta(0)$ are designated by θ_L and θ_0, respectively. $\theta_0 = \pi/2$.
δ_i	A right-handed rotation angle about $\hat{\mathbf{z}}_1$ from $\hat{\mathbf{x}}_1$ to a ray passing through the virtual primary backbone and the i*th* secondary backbone.
δ	$\delta \equiv \delta_1$ and $\delta_i = \delta + \beta_i$.
$\boldsymbol{\psi}$	$\boldsymbol{\psi} \equiv [\theta_L \ \ \delta]^T$ defines the configuration of the structure.

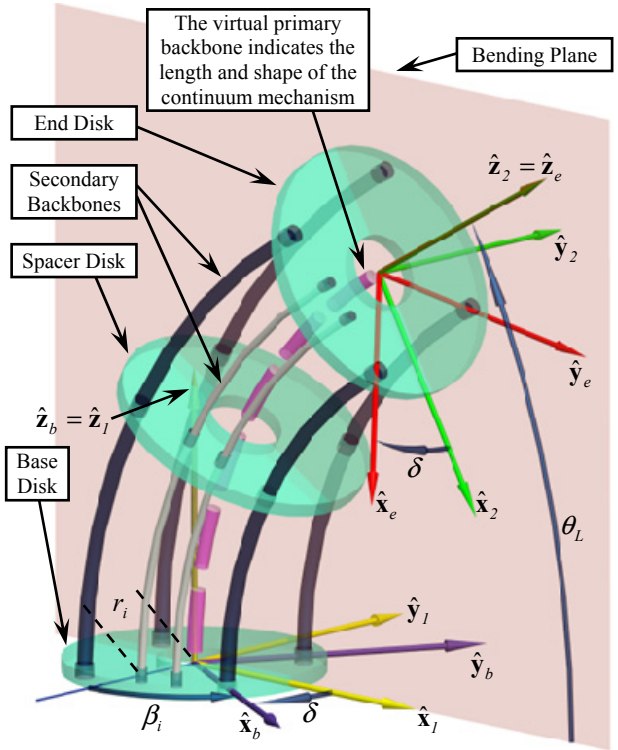

Fig. 5. Nomenclature and coordinates of the continuum mechanism

Thorough kinematics of similar continuum mechanism can be found in [20-22]. Related entities are summarized here.

Configuration of the mechanism is parameterized by $\boldsymbol{\psi}$ as defined in Table II. Projection of the i*th* secondary backbone on the bending plane is a curve which is offset by Δ_i from the primary backbone. $\rho(s)$ is related to $\rho_i(s_i)$ as follows:

$$\rho(s) = \rho_i(s_i) + \Delta_i \tag{3}$$

Where $\Delta_i \equiv r_i \cos\delta_i = r_i \cos(\delta + \beta_i)$ and each secondary backbone has its own values of r_i and β_i.

L and L_i are related according to:

$$L_i = \int ds_i = \int (ds_i - ds + ds) = L + \int (ds_i - ds) \tag{4}$$

Referring to Fig. 5, the integral above can be rewritten as in Eq. (5). Substituting Eq. (3) into Eq. (5) gives Eq. (6), which leads to the result as in Eq. (7):

$$\int (ds_i - ds) = \int_0^{\theta_0 - \theta_L} (\rho_i(s_i) - \rho(s)) d\theta \tag{5}$$

$$\int_0^{\theta_0 - \theta_L} (\rho_i(s_i) - \rho(s)) d\theta = -\int_0^{\theta_0 - \theta_L} \Delta_i d\theta \tag{6}$$

$$L_i = L - r_i \cos\delta_i (\theta_0 - \theta_L) = L + r_i \cos\delta_i (\theta_L - \theta_0) \tag{7}$$

Referring to the definition of q_i in Table II, Eq. (7) gives:

$$q_i = r_i \cos(\delta + \beta_i)(\theta_L - \theta_0), \ i = 1,2,\cdots,m \tag{8}$$

B. Synergy Implementation

When the continuum mechanism is bent, Eq. (8) holds for all the secondary backbones.

There are four driving secondary backbones in the mechanisms as shown in Fig. 6. Their structural parameters are listed in Table III (d_i, r_i, β_i, and $i = 1,2,3,4$). There are six driven backbones ($i = 5,6,\cdots,10$). Then the driving and the driven backbones are related as follows:

$$\begin{cases} q_1 = r_1 \cos(\delta + \beta_1)(\theta_L - \theta_0) \\ q_2 = r_2 \cos(\delta + \beta_2)(\theta_L - \theta_0), \ i = 5,6,\cdots,10 \\ q_i = r_i \cos(\delta + \beta_i)(\theta_L - \theta_0) \end{cases} \tag{9}$$

Using the numerical values of β_1 and β_2 listed in Table III, Eq. (9) can be simplified as follows:

$$\begin{cases} q_1 = r_1 \cos\delta(\theta_L - \theta_0) \\ q_2 = -r_2 \sin\delta(\theta_L - \theta_0) \\ q_i = r_i (\cos\delta\cos\beta_i - \sin\delta\sin\beta_i)(\theta_L - \theta_0) \end{cases} \tag{10}$$

$$q_i = \frac{r_i \cos\beta_i}{r_1} q_1 + \frac{r_i \sin\beta_i}{r_2} q_2, \ i = 5,6,\cdots,10 \tag{11}$$

It's clearly indicated by Eq. (11) that the length changes of the driven backbones q_i ($i = 5,6,\cdots,10$) are linear combinations of q_1 and q_2. The r_i and β_i of each driven secondary backbone can be obtained, solving the following two equations:

$$\begin{cases} \dfrac{r_i \cos\beta_i}{r_1} = u_{j1} \\ \dfrac{r_i \sin\beta_i}{r_2} = u_{j2} \end{cases}, \quad \begin{matrix} i = 5,6,\cdots,10 \\ j = 1,2,\cdots,6 \end{matrix} \tag{12}$$

Where u_{j1} and u_{j2} ($j = 1,2,\cdots,6$) are the corresponding elements of $\mathbf{u}_1$ and $\mathbf{u}_2$ from Table I.

The r_i and β_i values of all the driven backbones are solved and listed in Table III.

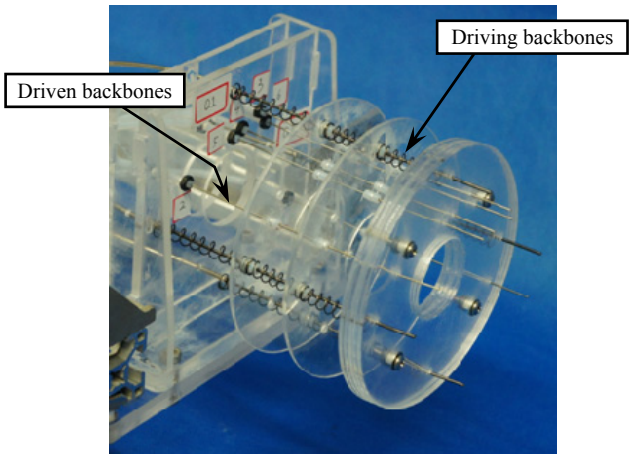

Fig. 6. The continuum mechanism for the synergy implementation

TABLE III
STRUCTURAL PARAMETERS OF THE CONTINUUM MECHANISM

Driving backbones	$r_i = 40mm$	$d_i = 1.2mm$	$i = 1,2,3,4$
	$\beta_1 = 0, \beta_2 = \pi/2, \beta_3 = \pi, \beta_4 = 3\pi/2,$		
Driven backbones	$d_i = 0.7mm$		$i = 5,6,\cdots,10$
$r_5 = 30.06mm$	$r_6 = 24.18mm$		$r_7 = 24.15mm$
$\beta_5 = 2.011\ rad$	$\beta_6 = -1.286\ rad$		$\beta_7 = 0.464\ rad$
$r_8 = 18.61mm$	$r_9 = 17.24mm$		$r_{10} = 22.18mm$
$\beta_8 = 0.151\ rad$	$\beta_9 = -0.070\ rad$		$\beta_{10} = 0.683\ rad$

IV. EXPERIMENTAL VERIFICATIONS

A series of experiments were carried out to demonstrate the effectiveness of the mechanical synergy implementation. The experimental setup is shown in Fig. 7.

The prosthetic hand has six NiTi rods for push-pull actuation. These actuation rods are routed through guiding cannulae made from PTFE to the continuum mechanism. The six actuation rods are connected to the driven backbones of the continuum mechanism via six locking blocks. These NiTi rod locking blocks also allow the adjustments of the lengths of the NiTi rods. Adjusting the lengths of the NiTi rods is equivalent to adjust the average pose of the prosthetic hand.

The four driving backbones of the continuum mechanism will be pushed and pulled according to the actuation kinematics as in Eq. (8). According to the β_i ($i = 1,2,3,4$) values listed in Table III, there is a π difference between β_1 and β_3, as well as between β_2 and β_4. Hence the actuation length q_1 is opposite to q_3, while q_2 is opposite to q_4. Two pinions (each meshed with two racks) are driven by two stepper motors to push and pull the driving backbones according to the actuation kinematics in Eq. (8). Driving backbones are routed from the racks to the continuum mechanism through rigid stainless steel channels, preventing buckling of the driving backbones.

The two stepper motors firstly stopped at the original positions ($g_1 = 0$ and $g_2 = 0$). At the original positions, the hand is in its average pose.

The motor g_1 was firstly commanded to move between -24.7 mm and +21.2 mm with the motor g_2 at zero position. The corresponding hand poses are shown in Fig. 8 and in the multimedia extension. Then the motor g_2 was commanded to move between -9.4 mm and +12.5 mm with the motor g_1 at zero position. The corresponding hand poses are also shown in Fig. 8 and in the multimedia extension.

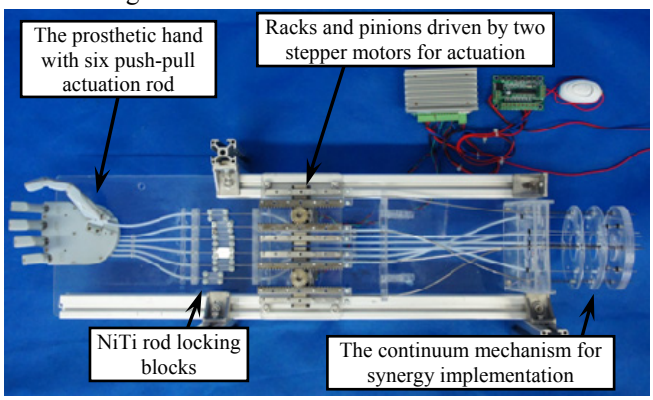

Fig. 7. Experimental setup for design verifications

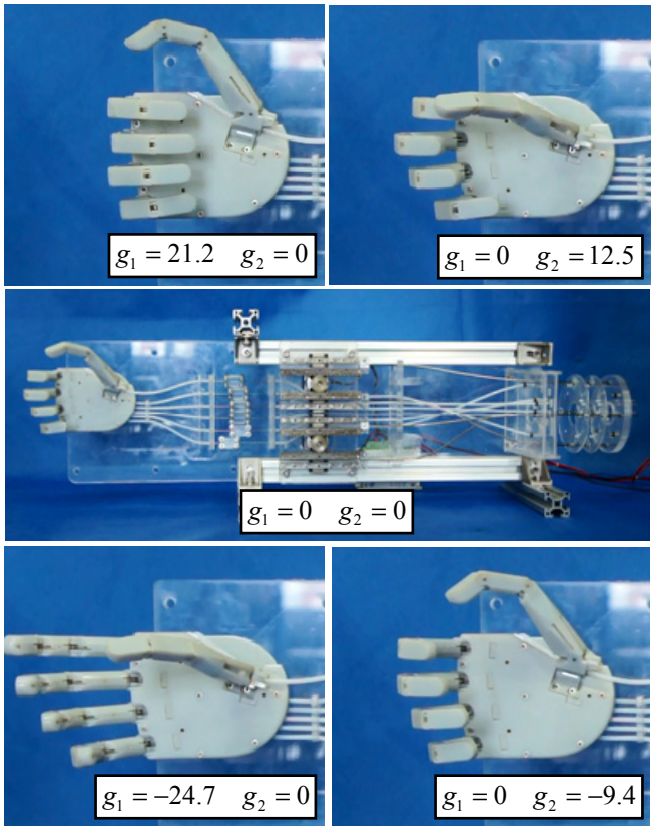

Fig. 8. Hand poses according to various inputs (g_1 and g_2) values

The g_{1i} and g_{2i} values from Table I were then used to drive the two stepper motors to realize the push-pull actuations of the driving backbones. The grasping poses were successfully regenerated, grasping the same objects as shown in Fig. 9 and in the multimedia extension.

V. CONCLUSIONS AND FUTURE WORK

When researchers design a prosthetic hand for various daily grasping tasks controllable via a few inputs, they often refer to the concept of postural synergy.

Instead of using multiple servomotors and implementing the postural synergies digitally in a controller, this paper proposes to implement the synergies mechanically using a simple continuum mechanism in order to eventually make such a synergy-based prosthetic hand more affordable.

Details about the hand design, the synergy synthesis and the continuum mechanism design are presented. Using the continuum mechanism, two independent translational inputs are scaled and combined to generate six translational outputs to drive the prosthetic hand. A series of experiments validated the proposed idea.

Future work would mainly be directed to explore other mechanism topologies to miniaturize the current continuum mechanism, in order to eventually embed two motors and the mechanical synergy implementation completely in hand.

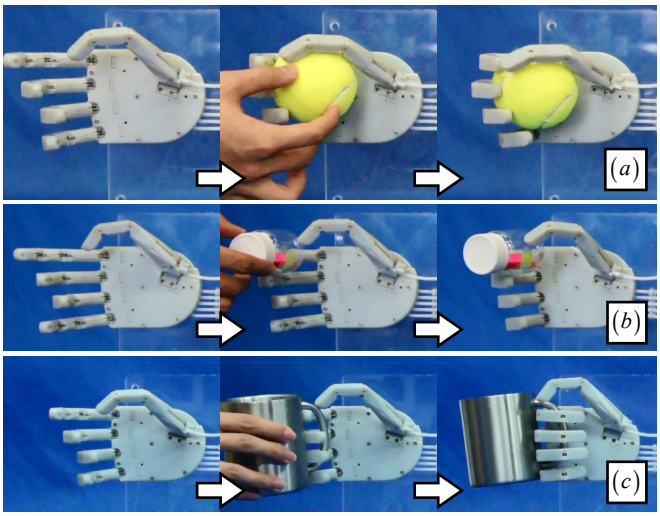

Fig. 9. Grasping poses realized using the g_{1i} and g_{2i} values from Table I: (a) a tennis ball, (b) a pill jar, (c) a mug

REFERENCES

[1] N. Bernstein, "The Problem of the Interrelation of Coordination and Localization," *Archives of Biological Sciences,* vol. 38, No.1, pp. 1-34, 1935.

[2] M. Santello, M. Flanders, and J. F. Soechting, "Postural Hand Synergies for Tool Use," *The Journal of Neuroscience,* vol. 18, No.23, pp. 10105-10115, Dec 1998.

[3] E. J. Weiss and M. Flanders, "Muscular and Postural Synergies of the Human Hand," *Journal of Neurophysiology,* vol. 92, No.1, pp. 523-535, 2004.

[4] A. Bicchi, "Hands for Dexterous Manipulation and Robust Grasping: a Difficult Road toward Simplicity," *IEEE Transactions on Robotics and Automation,* vol. 16, No.6, pp. 652-662, Dec 2000.

[5] J. P. Gazeau, S. Zeghloul, M. Arsicault, and J. P. Lallemand, "The LMS Hand : Force and Position Controls in the Aim of the Fine Manipulation of Objects," in *IEEE International Conf on Robotics and Automation (ICRA)*, Seoul, Korea, 2001.

[6] H. Liu, P. Meusel, N. Seitz, B. Willberg, G. Hirzinger, M. H. Jin, Y. W. Liu, R. Wei, and Z. W. Xie, "The Modular Multisensory DLR-HIT-Hand," *Mechanism and Machine Theory,* vol. 42, No.5, pp. 612-625, May 2007.

[7] M. Grebenstein, M. Chalon, W. Friedl, S. Haddadin, T. Wimböck, G. Hirzinger, and R. Siegwart, "The Hand of the DLR Hand Arm System: Designed for Interaction," *International Journal of Robotics Research,* vol. 31, No.13, pp. 1531-1555, 2012.

[8] T. Wimböck, B. Jahn, and G. Hirzinger, "Synergy Level Impedance Control for Multifingered Hands," in *IEEE/RSJ International Conference on Intelligent Robots and Systems (IROS)*, San Francisco, CA, USA, 2011, pp. 973-979.

[9] F. Ficuciello, G. Palli, C. Melchiorri, and B. Siciliano, "Experimental evaluation of Postural Synergies during Reach to Grasp with the UB Hand IV," in *IEEE/RSJ International Conference on Intelligent Robots and Systems (IROS)*, San Francisco, CA, USA, 2011, pp. 1775-1780.

[10] J. Rosell, R. Suárez, C. Rosales, and A. Pérez, "Autonomous Motion Planning of a Hand-Arm Robotic System Based on Captured Human-like Hand Postures," *Autonomous Robots,* vol. 31, No.1, pp. 87-102, 2011.

[11] E. Rombokas, M. Malhotra, and Y. Matsuoka, "Task-specific Demonstration and Practiced Synergies for Writing with the ACT Hand," in *IEEE International Conference on Robotics and Automation (ICRA)*, Shanghai, China, 2011, pp. 5363-5368.

[12] A. Zhang, M. Malhotra, and Y. Matsuoka, "Musical Piano Performance by the ACT Hand," in *IEEE International Conference on Robotics and Automation (ICRA)*, Shanghai, China, 2011, pp. 3536-3541.

[13] M. R. Cutkosky, "On Grasp Choice, Grasp Models, and the Design of Hands for Manufacturing Tasks," *IEEE Transactions on Robotics and Automation,* vol. 5, No.3, pp. 269-279, June 1989.

[14] T. Feix, R. Pawlik, H.-B. Schmiedmayer, J. Romero, and D. Kragić, "A Comprehensive Grasp Taxonomy," in *Robotics, Science and Systems Conference (RSS)*, Seattle, Washington, USA, 2009.

[15] J. Z. Zheng, S. De La Rosa, and A. M. Dollar, "An Investigation of Grasp Type and Frequency in Daily Household and Machine Shop Tasks," in *IEEE International Conference on Robotics and Automation (ICRA)*, Shanghai, China, 2011, pp. 4169-4175.

[16] M. T. Ciocarlie and P. K. Allen, "Hand Posture Subspaces for Dexterous Robotic Grasping," *The International Journal of Robotics Research,* vol. 28, No.7, pp. 851-867, June 2009.

[17] C. Y. Brown and H. H. Asada, "Inter-Finger Coordination and Postural Synergies in Robot Hands via Mechanical Implementation of Principal Components Analysis," in *IEEE/RSJ International Conference on Intelligent Robots and Systems (IROS)*, San Diego, CA, USA, 2007, pp. 2877-2882.

[18] K. Xu, J. Zhao, Y. Du, X. Sheng, and X. Zhu, "Design and Postural Synergy Synthesis of a Prosthetic Hand for a Manipulation Task," in *IEEE/ASME International Conference on Advanced Intelligent Mechatronics (AIM)*, Wollongong, Australia, 2013, pp. 56-62.

[19] K. Xu, Y. Du, H. Liu, X. Sheng, and X. Zhu, "Mechanical Implementation of Postural Synergies of an Underactuated Prosthetic Hand," in *Intl Conf on Intelligent Robotics and Applications (ICIRA)* Busan, Korea, 2013, pp. 463-474.

[20] K. Xu and N. Simaan, "An Investigation of the Intrinsic Force Sensing Capabilities of Continuum Robots," *IEEE Transactions on Robotics,* vol. 24, No.3, pp. 576-587, June 2008.

[21] K. Xu and N. Simaan, "Analytic Formulation for the Kinematics, Statics and Shape Restoration of Multibackbone Continuum Robots via Elliptic Integrals," *Journal of Mechanisms and Robotics,* vol. 2, No.011006, Feb 2010.

[22] R. J. Webster and B. A. Jones, "Design and Kinematic Modeling of Constant Curvature Continuum Robots: A Review " *International Journal of Robotics Research,* vol. 29, No.13, pp. 1661-1683, Nov 2010.